Non-uniform rf plasma potential due to edge asymmetry in large-area rf reactors

A. A. Howling, L. Sansonnens, J. Ballutaud, and Ch. Hollenstein
Centre de Recherches en Physique des Plasmas
Ecole Polytechnique Fédérale de Lausanne
PPH – Ecublens, CH-1015 Lausanne, Switzerland

J. P. M. Schmitt
Unaxis Displays, 5 Rue Léon Blum, F-91120 Palaiseau, France

In small area capacitive reactors, the rf and dc components of the plasma potential can be assumed to be uniform over all the plasma bulk because of the low plasma resistivity. In large area reactors, however, the rf plasma potential can vary over a long range across the reactor due to rf current flow and the non-zero plasma impedance. A perturbation in rf plasma potential, due to electrode edge asymmetry or the boundary of a dielectric substrate, propagates along the resistive plasma between capacitive sheaths. This is analogous to propagation along a lossy conductor in a transmission line, and the damping length of the perturbation can be determined by the telegraph equation. Some consequences are:

i) The spatial variation in sheath rf amplitudes causes non-uniform rf power dissipation near to the reactor sidewalls;

ii) The surface charge and potential of a dielectric substrate can be negative, and not only positive as for a uniform rf plasma potential. The variation of sheath dc potential across a dielectric substrate causes non-uniform ion energy bombardment;

iii) The self-bias voltage depends on the plasma parameters and on the reactor and substrate dimensions - not only on the ratio of electrode areas;

iv) The non-uniform rf plasma potential in presence of the uniform dc plasma potential leads to non-ambipolar dc currents circulating along conducting surfaces and returning via the plasma. Electron current peaks can arise locally at the edge of electrodes and dielectric substrates.

Perturbations to the plasma potential and currents due to the edge asymmetry of the electrodes are demonstrated by means of an analytical model and numerical simulations.

PACS numbers: 52.50.Dg, 52.80.Pi, 81.15.Gh

I. INTRODUCTION

Capacitively-coupled parallel plate rf reactors are commonly used for plasma enhanced chemical vapour deposition (PECVD) and dry etching of thin films such as amorphous silicon or silicon oxide. Large area (>1 m^2) reactors are used for the production of photovoltaic solar cells and thin film transistors for flat screens. These industrial applications typically require a uniformity in film thickness to better than ± 10%.

The plasma non-uniformity considered in this paper is due to the redistribution of rf current along the plasma near the edges of asymmetric electrodes, which is necessary to maintain rf current continuity. This results in non-uniform rf plasma potential and power dissipation, and consequently non-uniform deposition or etch rates. Moreover, it will be shown that the sheath dc potential can vary across a dielectric substrate resulting in non-uniform ion energy bombardment, a critical issue for uniformity of etch rate and material properties.

Many other phenomena can give rise to non-uniform deposition or etching in rf parallel plate reactors, including imperfect contact of the substrate with the electrode [1], inappropriate gas flow distribution [2], clouds of dust particles [3], and finite wavelength effects associated with high frequencies in large reactors [4–9]. In the first part of this work, it will be assumed for convenience that the rf frequency is low enough such that a quarter rf wavelength is much longer than the reactor dimensions. Conducting electrode surfaces are therefore equipotential for the dc and rf components over their whole surface. The case of high frequency in asymmetric reactors, which requires simultaneous treatment of both finite wavelength and edge effects, is briefly discussed in the appendix.

This paper is organised as follows: The basic edge asymmetry phenomenon is outlined in Section II. Section III develops a propagation model based on the telegraph equation [10] to show how the rf plasma potential is affected in large area reactors where the dimensions are larger than the damping length for rf voltage perturbations. Perturbations in potential and currents for a sequence of reactor configurations are then calculated by means of a simple analytical model. Comparisons with two numerical models are shown in Section IV. The consequences of non-uniform rf plasma potential are discussed in Section V before concluding.

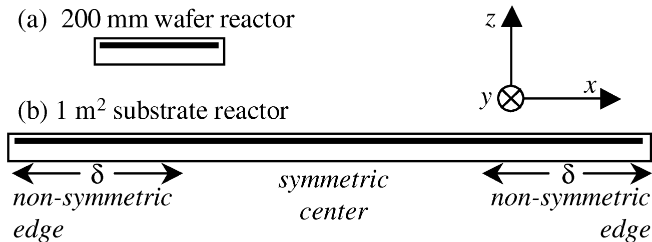

FIG. 1: Schematic scale view of two plasma processing reactors with a 25 mm electrode gap (taken from Schmitt *et al* [10]); (a) for a 200 mm wafer in a cylindrical reactor, and (b) for a 1 m^2 substrate in a rectangular reactor. The large-area reactor in (b) can be considered to have a central zone having symmetric electrodes, surrounded by asymmetric edge zones delimited by a characteristic damping length δ for rf current propagation.

II. FAILURE OF THE UNIQUE-PLASMA-POTENTIAL MODEL TO ACCOUNT FOR LARGE-AREA PLASMA REACTORS

The diagram in Fig. 1(a) shows a conventional asymmetric reactor where the inner, rf electrode area is less than the ground electrode area because of the grounded sidewalls used for lateral confinement of the plasma. Historically, rf reactors were sufficiently small so that the rf and dc plasma potentials could be taken to be the same over the entire plasma width: the plasma resistivity was low enough to 'short circuit' any plasma potential differences arising from the pattern of rf current flow to the sidewalls. For this case of a unique plasma potential, the uniform dc and rf sheath potentials and the dc self-bias of a capacitively-coupled rf electrode depend only on the ratio of electrode areas [11, 12].

For the large-area reactor in Fig. 1(b), however, the central zone could be considered to have symmetric electrodes (with plasma rf potential equal to half of the rf electrode voltage), whereas the edge zones apparently have non-symmetric electrodes (consequently with unbalanced rf sheath voltages). These different situations can be reconciled by postulating a variation of the rf plasma potential laterally across the reactor [10]. This perturbation arises because the supplementary rf current from the grounded sidewalls must be distributed across the plasma to the rf electrode to maintain rf current continuity. This re-distribution of rf current causes a perturbation to the rf plasma potential when the lateral plasma impedance is accounted for. The spatial profile of non-uniform rf plasma potential extends over a characteristic damping length δ which delimits the non-symmetric edge from the central symmetric region in Fig. 1(b). To summarize: for a non-symmetric reactor wider than the damping length, the rf sheath voltage amplitudes are unequal close to the reactor edges, but tend to be the same in the center as for a symmetric reactor.

For capacitively-coupled reactors, the dc current in the external circuit and transversely across the plasma is zero, but it will be shown in the following sections that, in the presence of non-uniform rf plasma potential, dc current circulates laterally *within* the plasma and returns via the conducting electrode surfaces of a large area reactor. It is only with the advent of reactors whose lateral dimensions exceed the damping length for rf potential perturbations (this defines 'large' in the context of this paper) that the inadequacies of the unique-plasma-potential model have become apparent. For example, the electrostatic charging of glass substrates is observed to be negative, and not positive as for a unique plasma potential situation [13]. It is shown below that the telegraph model can account for these observations.

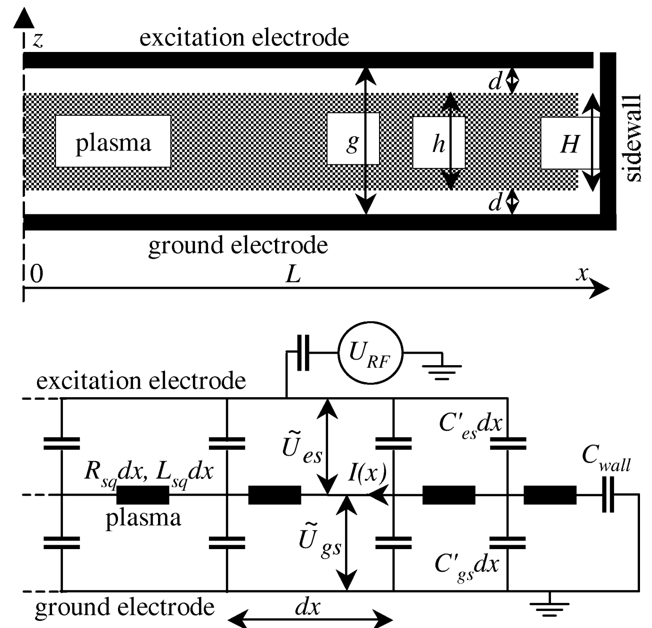

FIG. 2: Above: Schematic of the plasma reactor, showing a half-width L, with a grounded sidewall (not to scale). The electrode gap g contains a uniform bulk plasma, height h, with sheaths of thickness d so that $g = h + 2d$. The height H of the sidewall sheath in contact with the bulk plasma is $H = h$. Below: One-dimensional representation of the plasma equivalent circuit; es refers to the excitation electrode sheath, gs refers to the ground electrode sheath.

III. THE TELEGRAPH EQUATION APPLIED TO LARGE AREA RF REACTORS

In order to describe the propagation of a perturbation of the rf plasma potential in a large area reactor with non-zero plasma resistivity, we consider a one-dimensional equivalent circuit model of a uniform plasma slab with vacuum sheaths as shown in Fig. 2.

For this one-dimensional model, the plasma is taken to be infinitely long and uniform along the y direction (see Fig. 1). In the figure, C'_{gs} and C'_{es} represent the

ground and rf electrode sheath capacitance per unit area respectively, and $(R_{sq} + i\omega L_{sq})$ represents the *lateral* plasma sheet impedance per square, estimated as follows: In usual rf plasma processing conditions, where $\omega_{pe}^2 \gg \omega^2\big(1 + \nu_m^2/\omega^2\big)^{1/2}$, the conduction current in the plasma dominates the displacement current, and the plasma conductivity can be written as $\sigma_{pl} = \frac{n_e e^2}{m_e(i\omega+\nu_m)}$ [12] ($\omega_{pe} = \sqrt{\frac{n_e e^2}{\epsilon_0 m_e}}$ is the electron plasma frequency, n_e the plasma electron density, m_e the electron mass, ω the rf excitation angular frequency, and ν_m the electron-neutral collision frequency). For a uniform plasma slab of height h, the lateral plasma sheet impedance per square is $1/(\sigma_{pl} h) = R_{sq} + i\omega L_{sq}$, where R_{sq} is the dc sheet resistance, $R_{sq} = 1/(\sigma_{dc} h)$, ($\sigma_{dc} = \frac{n_e e^2}{m_e \nu_m}$ is the plasma dc conductivity), and $L_{sq} = R_{sq}/\nu_m$.

In the following, the transverse impedance of the bulk plasma is neglected in comparison with the sheath impedance. The transverse impedance of the bulk plasma is also small compared with the plasma lateral impedance because $h \ll L$. For a uniform plasma slab, and in absence of any perturbation, the rf potential amplitude across the ground sheath, $\tilde{U}_{gs}^0$, which is equal to the rf plasma potential $\tilde{U}_p^0$, is given by capacitive division:

$$\tilde{U}_{gs}^0 = \tilde{U}_p^0 = \tilde{U}_{rf} \frac{C'_{es}}{C'_{gs} + C'_{es}}, \tag{1}$$

where $\tilde{U}_{rf}$ is the rf excitation amplitude. In the absence of any dielectric substrate, $C'_{gs} = C'_{es} = \epsilon_0/d$ (where d is the vacuum sheath width) and the rf amplitude of the plasma potential is half of the rf excitation amplitude, as expected for equal, unit area electrodes.

In the presence of a perturbation $V(x,t)$ to the rf plasma potential (for example, due to the sidewall rf current), the time-dependent ground electrode sheath and plasma potentials become

$$\tilde{U}_{gs}(x,t) = \tilde{U}_p(x,t) = \tilde{U}_{gs}^0 \exp(i\omega t) + V(x,t), \tag{2}$$

and the excitation electrode sheath potential is

$$\tilde{U}_{es}(x,t) = \tilde{U}_{es}^0 \exp(i\omega t) - V(x,t), \tag{3}$$

where

$$\tilde{U}_{gs}^0 + \tilde{U}_{es}^0 = \tilde{U}_{gs}(x,t) + \tilde{U}_{es}(x,t) = \tilde{U}_{rf}. \tag{4}$$

A lateral rf current, $I(x,t)$ per unit length along y, (integrated over the plasma bulk height h) flows along the plasma to redistribute the rf current equally between the asymmetric electrodes, where (see Fig. 2):

$$\frac{\partial \tilde{U}_p}{\partial x} = \frac{\partial V}{\partial x} = -L_{sq}\frac{\partial I}{\partial t} - R_{sq} I \tag{5}$$

for the voltage drop due to lateral current flow, and

$$\frac{\partial I}{\partial x} = -C'_{gs}\frac{\partial \tilde{U}_{gs}}{\partial t} - C'_{es}\frac{\partial \tilde{U}_{es}}{\partial t} = -C'\frac{\partial V}{\partial t} \tag{6}$$

for continuity of the lateral current, where $C' = C'_{gs} + C'_{es} = 2\epsilon_0/d$ is the combined parallel sheath capacitance per unit area. The voltage perturbation is therefore given by

$$\frac{\partial^2 V}{\partial x^2} - L_{sq}C'\frac{\partial^2 V}{\partial t^2} - R_{sq}C'\frac{\partial V}{\partial t} = 0. \tag{7}$$

which is the telegraph equation. The lateral current flow along the plasma between the sheaths which isolate the plasma from the electrodes is analogous to current flow down a transmission line which has a lossy conductor; the sheaths represent the dielectric medium of the line. The name "telegraph equation" specifically applies to signal transmission down a lossy transmission line.

The voltage perturbation due to the sidewall in Fig. 2 has the same frequency as the rf excitation, so $V(x,t) = V(x)\exp(i\omega t)$. The general solution for the voltage perturbation in Eq. 7 is

$$V(x,t) = V_1 \exp(\gamma x)\exp(i\omega t) + V_2 \exp(-\gamma x)\exp(i\omega t), \tag{8}$$

where γ is the propagation factor given by

$$\gamma^2 = (i - \omega/\nu_m)\omega R_{sq} C', \tag{9}$$

and we have substituted for $L_{sq} = R_{sq}/\nu_m$. For low excitation frequency and high pressure, $\omega/\nu_m \ll 1$ (for example, $\omega/\nu_m \approx 0.1$ for 13.56 MHz and 0.2 mbar in argon), and the sheet inductive impedance ωL_{sq} can be neglected with respect to R_{sq} for convenience, giving:

$$\gamma \approx \frac{(1+i)}{\delta};\ \delta = \sqrt{\frac{2}{\omega R_{sq} C'}} = \sqrt{\frac{\sigma_{dc} h d}{\omega \epsilon_0}} = \omega_{pe}\sqrt{\frac{hd}{\omega \nu_m}} \tag{10}$$

by substitution for R_{sq} and C'. The solution for the perturbation to the plasma rf potential propagating along the x direction is therefore of type

$$V = V_1 e^{-x/\delta} e^{i(\omega t - x/\delta)}, \tag{11}$$

which is a strongly damped wave with $1/e$ damping length δ and wavelength $2\pi\delta$. The effect of inductance is to increase the damping length and decrease the wavelength. Values of δ were estimated for various pressures and electron densities in Fig. 3. The damping length can easily be smaller than the dimensions of PECVD reactors, and consequently any non-uniform rf plasma potential, due to discontinuities such as the edges of electrodes and dielectric boundaries, will extend across the substrate resulting in a non-uniform plasma process.

For the purposes of the following analytical description, we will assume that the plasma density and temperature are unaffected by the spatial variation of the voltage perturbation, which is a reasonable first order approximation if $|V(x,t)| \ll \tilde{U}_{rf}$. This model is therefore not a self-consistent description and is only intended to give a physical picture of the various edge effects. A self-consistent treatment is left to the numerical modeling

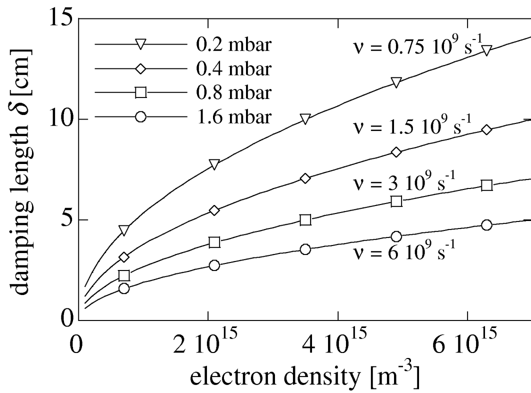

FIG. 3: Estimated damping length δ, at 13.56 MHz excitation frequency, as a function of electron density for four values of the electron-neutral collision frequency. Approximate equivalent pressures for argon are given in the legend. For the examples shown in this work, the plasma height is 19 mm and the sheath widths are 3 mm for a total electrode gap of 25 mm.

in Section IV. We now develop five illustrative examples, progressing systematically towards a realistic experimental configuration, in the following sequence:

III A Asymmetric reactor with insulating electrodes;

III B Asymmetric reactor with conducting electrodes;

III C Asymmetric conducting reactor with a thin dielectric substrate;

III D Symmetric conducting reactor with a thick dielectric substrate;

III E Asymmetric conducting reactor with a thick dielectric substrate.

The procedure for each example will be the same as follows:

i) the telegraph equation is used to calculate the spatial profile of the plasma rf potential amplitude;

ii) the condition for zero net dc current to the ground electrode is used to deduce the dc plasma potential;

iii) the condition for zero net dc current to the rf excitation electrode is then used to deduce the dc self-bias voltage.

Finally, in Section III F, it is shown how the telegraph effect can be eliminated using a symmetric reactor design.

1-D Cartesian geometry is used, which assumes that the reactor dimension along y in Fig. 1 is infinitely long so that the influence of the reactor corners and lateral walls parallel to the x axis can be neglected. For a real reactor, the telegraph equation can be solved for two dimensions, x and y [14].

A. Asymmetric reactor with a thin insulating film on the electrodes

The reactor asymmetry in Fig. 2 is due to the grounded vertical sidewalls at $x = \pm L$. The solution of Eq. 7, using Eq. 2 for the rf plasma potential, is an even function in x:

$$\tilde{U}_p(x) = \tilde{U}^0_{gs} + V_1 \exp(\gamma x) + V_1 \exp(-\gamma x) = \tilde{U}^0_{gs}\Big[1 - K\cosh(\gamma x)\Big], \quad (12)$$

where the constant K remains to be determined by the boundary condition at the sidewalls. There is no dielectric substrate, therefore the sheath capacitances per unit area are equal in Eq. 1 and so $\tilde{U}^0_{gs} = \tilde{U}_{rf}/2$.

The capactive coupling of the plasma via the sidewall sheath, height H, to the sidewall causes a perturbation to the rf current of

$$I_{wall} = C_{wall}\frac{\partial \tilde{U}_p(L,t)}{\partial t} = i\omega C_{wall}\tilde{U}_p(L) \quad (13)$$

for unit length of the sidewall along y. If we assume for convenience that the sheath between the plasma and the sidewall has the same width as for the electrodes, then $C_{wall} = C'_{gs}H = C'H/2$. The boundary condition is satisfied by equating the current in Eq. 13 with the current at $x = L$ from Eq. 5 (with $L_{sq} = 0$), which gives K. The spatial profile envelope of the plasma rf potential amplitude is then given by the magnitude of

$$\tilde{U}_p(x) = \frac{\tilde{U}_{rf}}{2}\Big[1 - K\cosh(\gamma x)\Big]; \qquad K = \frac{H}{(2/\gamma)\sinh(\gamma L) + H\cosh(\gamma L)}. \quad (14)$$

The ground sheath rf voltage profile $\tilde{U}_{gs}(x)$ is identical to Eq. 14 and the equivalent profile for the rf electrode sheath, $\tilde{U}_{es}(x)$, is obtained from $\tilde{U}_{gs} + \tilde{U}_{es} = \tilde{U}_{rf}$.

The relative non-uniformity in plasma potential can be represented as the magnitude of $\frac{U_p(O)-U_p(L)}{U_{rf}/2}$. This non-uniformity extends into the plasma over about $\pi\delta$ from the reactor wall. In Fig. 4(a) with a fixed reactor size, the smaller the value of δ, the stronger the non-uniformity and the more closely it is confined to the reactor walls. In Fig. 4(b), for sufficiently large reactors, the degree of non-uniformity is independent of L; for such a reactor with halfwidth $L > \pi\delta$, the relative plasma potential non-uniformity is given by $\left[2(\delta/H)^2 + 2(\delta/H) + 1\right]^{-1/2}$ which depends only on the ratio of damping length to the length of the sidewall sheath.

An example of the sheath potential profiles is given in Fig. 5(a) for a 50 cm wide reactor and δ=5 cm, where the transition from the unequal sheath potentials at the asymmetric edge to the almost-symmetric sheaths at the center is shown. The sheath potentials vary by about 22 %, and this perturbation extends inwards from the walls over a distance of about 15 cm.

Since the electrode surfaces in this sub-section are insulating, they will charge up to the dc sheath self-rectification voltage [15–17] necessary to maintain local ambipolarity (zero dc current) everywhere. For the ground electrode this is given by

$$\bar{U}_{gs} = U_f + T_e \ln[\mathbf{I}_0(|\tilde{U}_p|/T_e)] \quad (15)$$

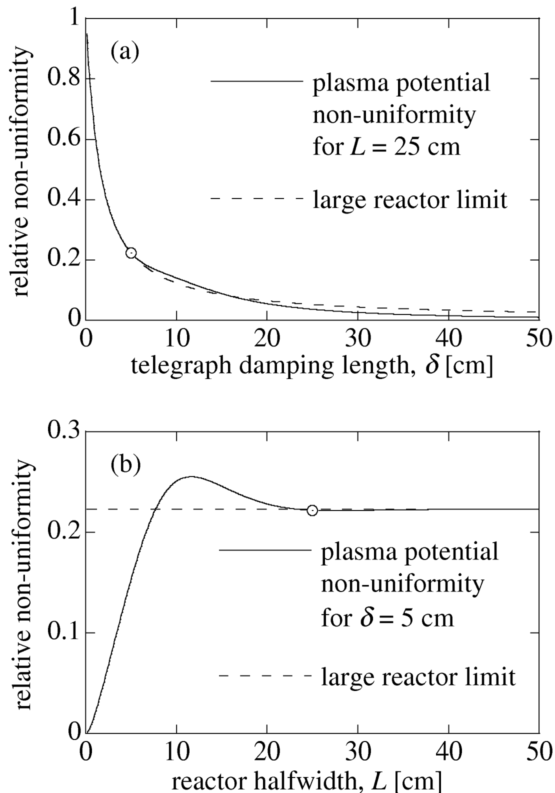

FIG. 4: The relative non-uniformity in plasma potential, for H =19 mm: a) as a function of the damping length δ, for L = 25 cm and for the limit of a large reactor; b) as a function of reactor halfwidth L, for δ = 5 cm. The dashed lines correspond to the expression for large reactors given in the text. The points indicated correspond to the parameters used for the following examples in this paper, namely L = 25 cm and δ = 5 cm.

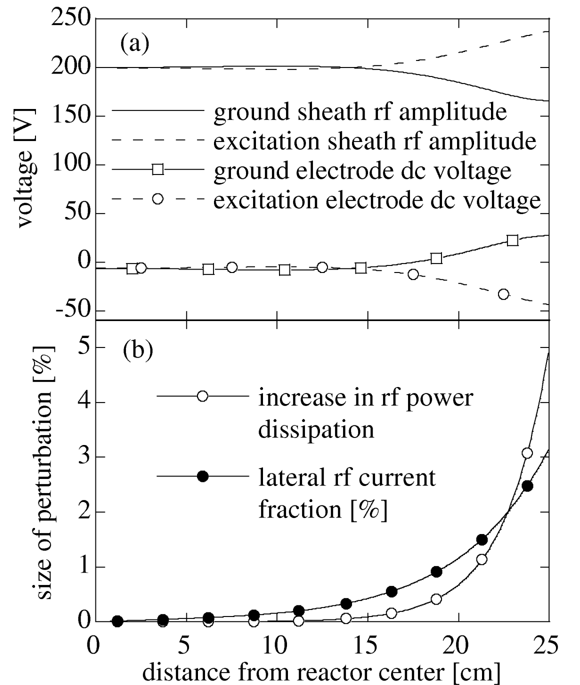

FIG. 5: a) Calculated envelope of the magnitude of the sheath rf potentials at the ground and excitation electrodes in an asymmetric reactor, halfwidth L = 25 cm, with plasma height $h = H$ = 19 mm and rf voltage amplitude 400 V. The damping length is δ = 5 cm. The transition from the asymmetric edge to symmetric center is clearly shown. Also shown are the time-averaged potentials on the ground and excitation *insulating* electrodes for T_e = 3 eV - the electrode surfaces charge up to maintain local ambipolarity; b) the relative increase in total rf plasma power at the edge, assuming power dissipation proportional to the sum of the squares of the rf sheath voltages, and magnitude of the rf *lateral* current perturbation normalised to the *transverse* rf discharge current.

for a sinusoidal sheath voltage, where $\mathbf{I}_0$ is the zeroth order modified Bessel function and $U_f = \frac{T_e}{2}\ln(M_i/2.3m_e)$ is the voltage difference of a floating probe in a dc plasma below the plasma potential. The magnitude of the plasma rf potential is used since the phase has no significance for time-averaged, dc values. The corresponding electrode surface voltages are shown in Fig. 5(a). The time-averaged current is zero everywhere, and therefore the plasma dc potential is uniform (equipotential), taken to be $\tilde{U}_{rf}/2$ = 200 V in the example shown. The ground electrode surface dc potential becomes more positive towards the edges because the self-rectification voltage is smaller, compared to the dc plasma potential, in presence of the reduced rf amplitude of the ground sheath.

Figure 5(b) shows the total edge power dissipation which increases by about 5 % relative to the unperturbed value, assuming power dissipation proportional to the sum of the square of the rf sheath voltages. Note that, because of the 22 % variation in the individual rf sheath voltages in Fig. 5(a), the increase in the excitation electrode sheath power at the edge is 49 % above the unperturbed value, and 39 % less power at the edge of the ground electrode sheath with respect to the unperturbed value.

From Eq. 5 or 6, the lateral rf current perturbation I can be calculated. When normalised to the rf plasma (transverse) current $I_0 = i\omega LC'U_{rf}/2$ per unit length along y, we obtain:

$$\frac{I}{I_0} = \left(\frac{1}{\gamma L}\right) K \sinh(\gamma x), \qquad (16)$$

whose magnitude is about 3 % in the example of Fig. 5(b), being largest at the edges and falling to zero at the center, as expected because the edge sidewalls are the source of the rf current perturbation.

B. Asymmetric reactor with conducting electrodes

The reactor geometry is the same as in Fig. 2, and so the solutions for the envelopes of the sheath rf voltage amplitudes are the same as in Eq. 14 and Fig. 5(a).

However, now the dc potential of the conducting electrodes, the dc plasma potential $\bar{U}_p$ and therefore the dc sheath voltages are all uniform. Since the rf amplitude varies with position, however, there are now regions where the dc and rf sheath voltages do not satisfy the self-rectification condition in Eq. 15 for zero dc current, resulting in local non-ambipolar dc current flow. The dc current density from the plasma to the ground electrode is given in terms of $\tilde{U}_p(x)$ and $\bar{U}_p$ by [15]:

$$j_{dc} = j_{sat}\left[1 - \mathbf{I}_0(|\tilde{U}_p|/T_e)\exp\left(\frac{U_f - \bar{U}_p}{T_e}\right)\right], \quad (17)$$

where j_{sat} is the saturated ion current density [12]. Ion current from the plasma to the electrodes is defined as positive in this work. The surface-integrated dc current flow is zero for each electrode, as imposed by the capacitive coupling: The constraint of zero net dc current to the ground electrode, $\int_0^L j_{dc}\,dx + Hj_{dc(x=L)} = 0$ (which includes the dc current to the sidewall), using Eq. 17, determines the dc plasma potential $\bar{U}_p$. The constraint of zero net dc current to the excitation electrode is obtained by a similar integral (excluding sidewall) for the excitation electrode sheath with rf voltage $\tilde{U}_{es} = \tilde{U}_{rf} - \tilde{U}_p$ and dc voltage $\bar{U}_{es} = \bar{U}_p - \bar{U}_{sb}$, which determines the self-bias $\bar{U}_{sb}$. Dc current is therefore constrained to flow in to and out of each electrode sheath, circulating via the plasma and the conducting surface of the electrode. The result is that asymmetry in large reactors leads to circulating dc currents. The spatial profiles of dc current flow across the sheaths, using Eq. 17, are shown in Fig. 6(a) along with a schematic of the circulating dc current in Fig. 6(b). In Fig. 6(b), a net positive time-averaged dc current in Fig. 6(a) is represented as a net flow of positive ions from the plasma to the corresponding electrode; similarly, a net negative dc time-averaged current is represented as a net flow of electrons from the plasma to the corresponding electrode. The dc current densities are given in units of saturated ion current density, j_{sat}, and the integrated dc currents flowing along the electrode surfaces (per unit length along y) are in units of j_{sat}m. The dc plasma potential is $\bar{U}_p$ = 206 V, and the self-bias $\bar{U}_{sb}$ = -28 V.

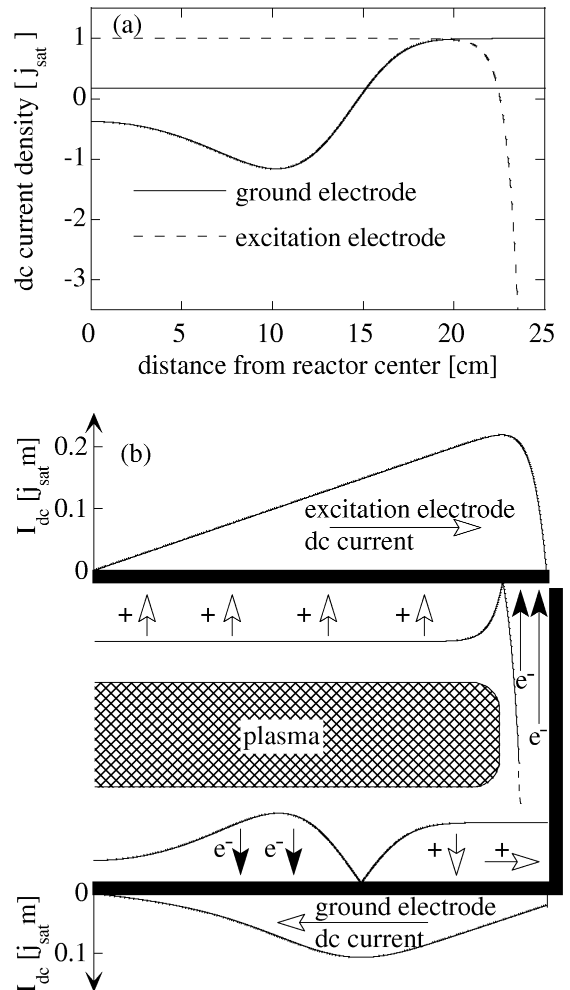

FIG. 6: a) Calculated dc current flow across the sheaths of the ground and excitation electrodes (zero net dc current to each electrode) in an asymmetric *conducting* reactor (same dimensions as Fig. 5); b) schematic representation of the corresponding circulating currents. This is the dc current circulation caused by the reactor asymmetry in Fig. 2. Ion current from the plasma to the electrodes is defined as positive.

Since there are dc as well as rf currents, there is no *a priori* reason why the dc plasma potential $\overline{U}_p$ should, in fact, be equipotential, because the rf and dc resistivities are the same in the limit $\omega/\nu_m \ll 1$ chosen for convenience in this work. A self-consistent plasma model, as in Section IV, would also take the spatial variation of $\overline{U}_p$ into account. However, since the dc currents are generally limited by the ion saturation current, except where strong localized electron currents arise, the dc currents and lateral voltage variations are much less than the rf currents and voltages, and the time-averaged plasma potential is therefore taken to be spatially uniform in this work for simplicity. Measurements of the dc currents can serve as diagnostics for experimental verification of the telegraph effect [14].

Because the plasma density is assumed to be constant throughout the whole reactor, and not influenced by the spatial variation of rf sheath voltage (reasonable if $V(x,t) \ll \tilde{U}_{rf}$), the intense peaks of electron current at the edges of the rf electrode are due entirely to the non-uniform rf plasma potential in this model, and not due to zones of intense power disspiation due to edge-localized fields as, for example, in Refs. [7, 18].

Due to the high electron mobility, the plasma potential will tend to remain positive with respect to all *conducting* electrode surfaces. In the limit where the rf voltage is much larger than T_e, the dc sheath potential will therefore always be approximately equal to the maximum of the envelope of rf amplitude (due to self-rectification [17]). Consequently, the dc plasma potential will be approximately equal to the ground sheath rf amplitude in the central, symmetric zone of the reactor, i.e. $\bar{U}_p \approx \tilde{U}_{gs}(x = 0)$. In contrast, the rf amplitude of the

sheath potential of the excitation electrode increases towards the edge, $x = L$, and so its dc sheath voltage must increase accordingly. This can only be accomplished by driving the dc voltage of the excitation electrode to a negative self-bias value. In the limit $\tilde{U}_{rf} \gg T_e$, the self-bias $\bar{U}_{sb}$ tends to the difference between the largest values of the sheath self-rectification voltages:

$$\bar{U}_{sb} \approx \tilde{U}_{gs}(x=0) - \bar{U}_{es}(x=L). \tag{18}$$

Substituting the expressions for the rf sheath amplitudes in section III A, the self-bias can be estimated from:

$$\bar{U}_{sb} \approx -|\frac{\tilde{U}_{rf}}{2} K(1 + \cosh \gamma L)|, \tag{19}$$

which is negative as expected for a reactor with excitation electrode smaller than the ground electrode [11]. The self-bias for a *small* reactor (i.e. with unique plasma potential as described in Section II), in the same limit of $U_{rf} \gg T_e$, depends only on the sheath capacitances [11] and is given by $\bar{U}_{sb} = \frac{C_{es}-C_{gs}}{C_{es}+C_{gs}} = -\tilde{U}_{rf}\left(\frac{H}{2L+H}\right)$, since $C_{es} = \epsilon_0 2L/d$ and $C_{gs} = \epsilon_0(2L+2H)/d$ in the model used here. This corresponds to the limit of Eq. 19 for $L \ll \delta$, as expected because this defines a small reactor in the context of this work. The dependence on δ of Eq. 19 is indicated Fig. 7(a), and on L in Fig. 7(b). Compared to the conventional unique-plasma-potential model relevant to small reactors, the telegraph model predicts that the self-bias voltage in a large reactor can be more negative and depends on reactor geometry and damping length, and not only on the ratio of sheath capacitances.

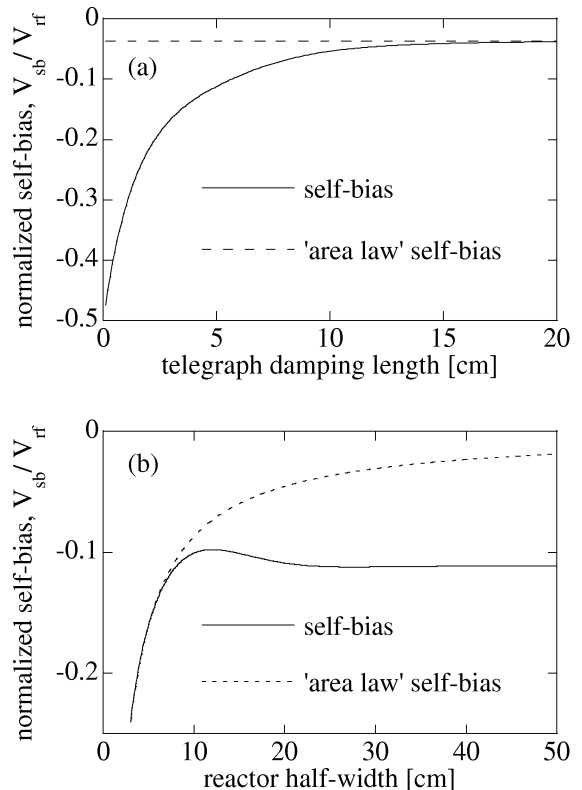

FIG. 7: (a) The dependence of self-bias, normalised to the rf voltage amplitude, on the damping length for a reactor of halfwidth $L = 25$ cm and plasma height $h = H = 19$ mm. In the limit of long damping length, the self-bias tends towards the value given by the area law, which depends on L, h and not δ. (b) The dependence of self-bias, normalised to the rf voltage amplitude, on reactor half-width for a given damping length of $\delta = 5$ cm and plasma height $h = H = 19$ mm. In the limit of a wide reactor, the self-bias depends on the edge zone determined by hH, δ and not L; this is different from the area law.

C. Asymmetric conducting reactor with a thin dielectric substrate

We now consider the effect of a thin dielectric substrate placed symetrically on the ground electrode, width $2S$ ($S < L$), as in Fig. 8(c). By 'thin dielectric' it is meant that the capacitive impedance of the dielectric is negligible compared with the sheath impedance, in which case the dielectric substrate does not alter the rf current distribution in the reactor. Consequently, the envelopes of the sheath rf voltage amplitudes are again the same as in Eq. 14 and Fig. 5(a), as for sections III A and III B. However, global ambipolarity for the ground electrode now concerns the dc current only near to the reactor edge, beyond the substrate. The surface integral of the time-averaged ground sheath current is now performed for the sidewall and $S < x < L$ only. The modified values of the dc potentials and currents are shown in Fig. 8(a) and (b). For a physical interpretation of these figures, we note that the dc plasma potential is constrained to decrease to 184 V (from 206 V), being approximately equal to the rf ground sheath amplitude at the edge of the substrate which now defines the maximum rf amplitude above the conducting surface, so that

$$\bar{U}_p(x) = \bar{U}_{gs}(x) \approx |\frac{\tilde{U}_{rf}}{2}\left[1 - K\cosh(\gamma S)\right]|. \tag{20}$$

In order to compensate the positive ion current to the grounded sidewall and electrode, a localized peak of electron current from the plasma to the electrode arises near to the boundary of the substrate, as shown in Figs. 8(b) and (c). The rf sheath voltage at the excitation electrode is unchanged, and therefore, since the dc plasma potential has decreased, the self-bias is driven to a more negative value by a similar amount, to -49 V (from -28 V). Eq. 19 becomes

$$\bar{U}_{sb} \approx -|\frac{\tilde{U}_{rf}}{2}\left[K(\cosh(\gamma S) + \cosh(\gamma L))\right]|. \tag{21}$$

In contrast, since the rf current continuity is identical for the reactors in sections III A and III B, the conventional

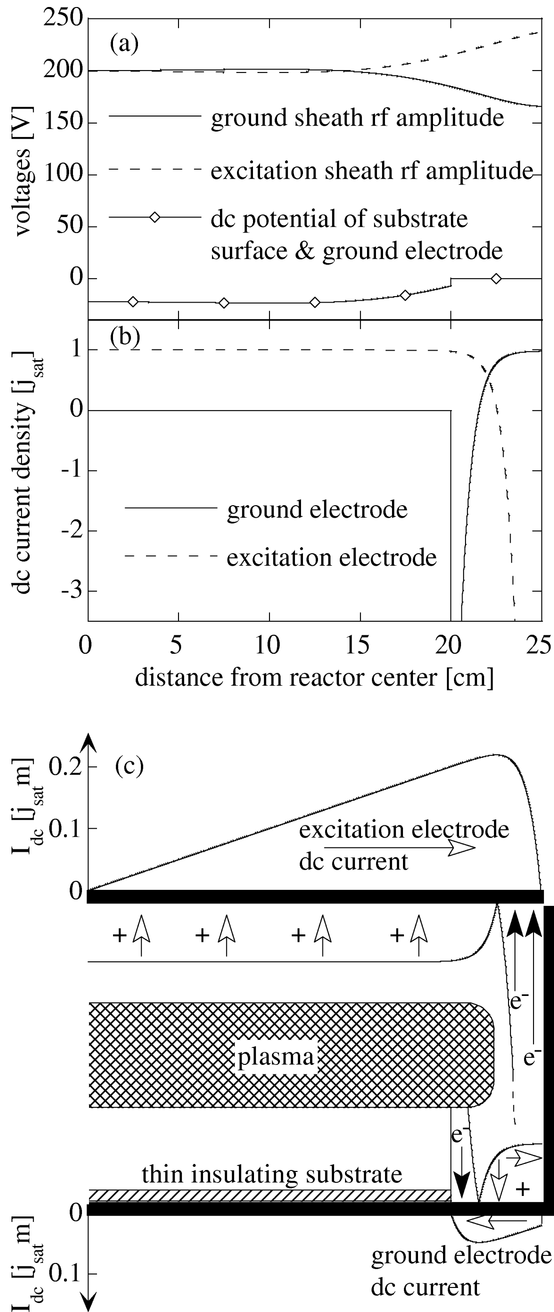

FIG. 8: a) Calculated rf sheath voltage amplitudes and dc potential of the substrate surface as for the case in section III B, but with a thin dielectric substrate on the ground electrode of halfwidth 20 cm; b) estimated dc current flow as modified by the thin dielectric substrate; and c) schematic representation of the corresponding circulating dc currents.

self-bias calculation [11] would predict that the self-bias is the same, i.e. independent of the thin substrate.

The insulating substrate surface charges up to reach the dc sheath voltage necessary for local ambipolarity according to Eq. 15. However, because the rf ground sheath potential is unchanged with respect to the previous sections, whereas the dc plasma potential is now reduced, a surprising consequence is that the substrate surface becomes *negatively* charged to maintain local ambipolarity - this effect has been observed experimentally by measuring a negative substrate charge [13]. This negative polarity would be impossible to explain in the context of a unique-plasma-potential model, because capacitive division between the positive plasma potential and the substrate surface would otherwise always lead to a positive substrate potential and a positive surface charge. The experimental observation of negative substrate charge is strong support for a spatially-varying rf plasma potential description such as the telegraph model.

D. Symmetric conducting reactor with a thick dielectric substrate

A thick dielectric substrate on the ground electrode reduces the unit area capacitance of plasma to ground, C'_{gs}, due to capacitive division between the vacuum sheath and the substrate. There are two consequences in this 1D telegraph model, namely an increase in the equilibrium rf plasma potential, $\tilde{U}^0_{gs}$ (Eq. 1), and an increase in the damping length δ (Eq. 10). We will illustrate the effect of the thick substrate by first considering the substrate in a hypothetical reactor with no sidewalls (H=0 and therefore C_{wall}=0 in Eq. 13) as in Fig. 9(c).

For a dielectric substrate of thickness t and relative permittivity ϵ_r, the series capacitance of the substrate and sheath (with assumed constant thickness d) is reduced by a factor $(1 + t/d\epsilon_r)$ and the equilibrium rf plasma potential is increased from $\tilde{U}^0_{gs} = \tilde{U}_{rf}/2$ by an amount $F\tilde{U}_{rf}/2$ where $F = (1 + 2d\epsilon_r/t)^{-1}$. The damping length δ_S is longer than δ by a factor $\sqrt{(1 + F)}$. By matching the rf plasma potential and lateral rf current at the boundaries of the substrate, $x = \pm S$, the rf plasma potential profile within $(0 \le x \le S)$ and beyond $(S \le x \le L)$ the substrate area are:

$$\tilde{U}_p(x) = \frac{\tilde{U}_{rf}}{2}\left[1 + F - K_{0S}\cosh(\gamma_S x)\right] \text{ for } 0 \le x \le S, \tag{22}$$

and

$$\tilde{U}_p(x) = \frac{\tilde{U}_{rf}}{2}\left[1 + K_{SL}\cosh(\gamma(L - x))\right] \text{ for } S \le x \le L, \tag{23}$$

where

$$K_{0S} = \frac{F\sinh(\gamma D)}{\cosh(\gamma_S S)\sinh(\gamma D) + (\gamma_S/\gamma)\sinh(\gamma_S S)\cosh(\gamma D)} \tag{24}$$

and

$$\frac{K_{SL}}{K_{0S}} = \left(\frac{\gamma_S}{\gamma}\right)\frac{\sinh(\gamma_S S)}{\sinh(\gamma D)}. \tag{25}$$

$D = L - S$ is the gap between the substrate edge and the reactor edge. The corresponding profiles for rf current

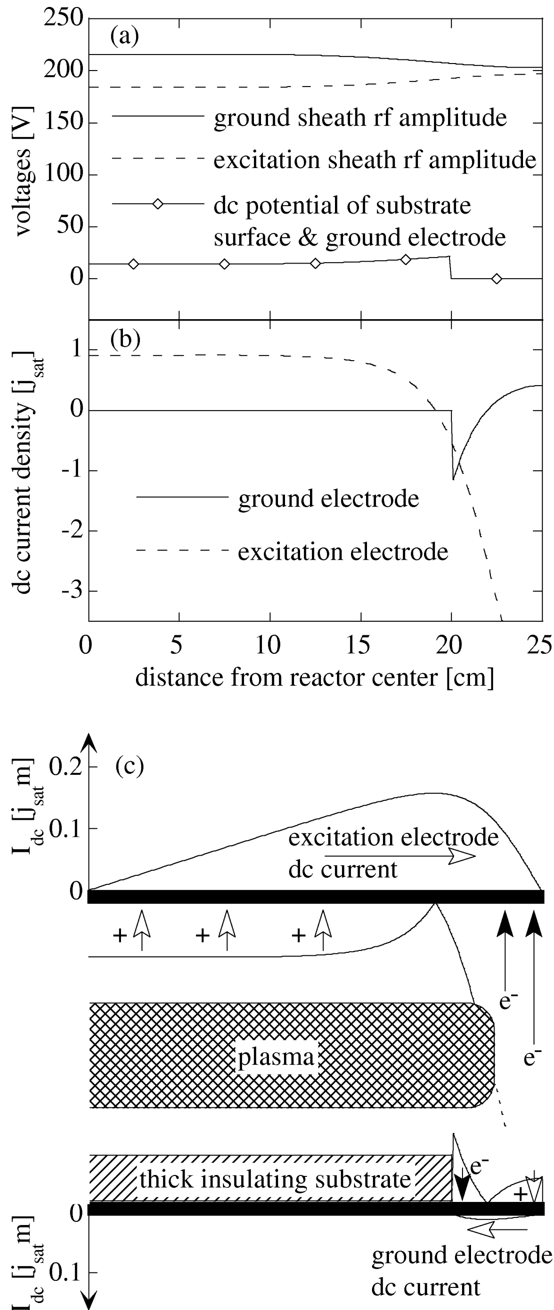

FIG. 9: For a thick dielectric substrate (3 mm thick, relative permittivity $\epsilon_r = 6$, corresponding to glass) in a hypothetical *symmetric* reactor with no sidewalls: a) Sheath rf voltage amplitudes and dc potential of the substrate surface; b) calculated dc current flow; c) schematic representation of the corresponding circulating dc currents.

amplitude, dc potentials and dc current circulation are shown in Fig. 9. The sheath rf voltages are now unequal above the thick substrate, and tend towards equality at the symmetric edge of the reactor. The dc plasma potential is 211 V. Note that the dc voltage on the substrate surface this time is determined from Eq. 15 using the rf voltage across the ground *sheath*, not the rf plasma potential. The ground sheath rf voltage is reduced due to capacitive division with the thick dielectric substrate, which leads to a reduction in the ground sheath dc voltage required for local ambipolarity (using Eq. 15), and the substrate voltage is consequently always positive for this case of a reactor without sidewalls. The discontinuity in the dc potential of the ground electrode surface in Fig. 9(a) at the substrate edge is likewise due to the abrupt change in sheath rf amplitude, in the presence of a continuous plasma-to-ground rf amplitude envelope.

Note that the self-bias, +13 V, is also positive because the effective capacitance to ground is now less than the capacitance to the excitation electrode [11], even though the electrode areas are the same. The non-uniform profile of rf plasma potential amplitude, in the presence of the equipotential dc plasma, leads to the circulating dc currents as shown in Fig. 9(c).

E. Asymmetric conducting reactor with a thick dielectric substrate

The configuration shown in Fig. 10(c) is closest to a typical situation for reactors used for PECVD and etching. The analytical treatment is complicated by the opposing changes to the plasma-to-ground sheath capacitance (it is larger due to the grounded sidewall, but smaller due to the thick dielectric substrate), and the many independent parameters $(H, L, S, t/\epsilon_r, d, \delta)$. Fortunately, it is only necessary to combine the modelling steps outlined in the preceding sections. The boundary condition at $x = L$ accounts for the sidewall current, and the internal boundary at $x = S$ requires continuity of voltage and current at the substrate edge. The solution for the rf plasma potential amplitude, shown in Fig. 10(a), is:

$$\tilde{U}_p(x) = \frac{\tilde{U}_{rf}}{2}\left[1 + F - K'_{0S}\cosh(\gamma_S x)\right] \text{ for } 0 \leq x \leq S, \tag{26}$$

and

$$\tilde{U}_p(x) = \frac{\tilde{U}_{rf}}{2}\Bigg[1 + K'_{SL}\cosh(\gamma(x-S)) - K''_{SL}\sinh(\gamma(x-S))\Bigg] \text{ for } S \leq x \leq L \tag{27}$$

where

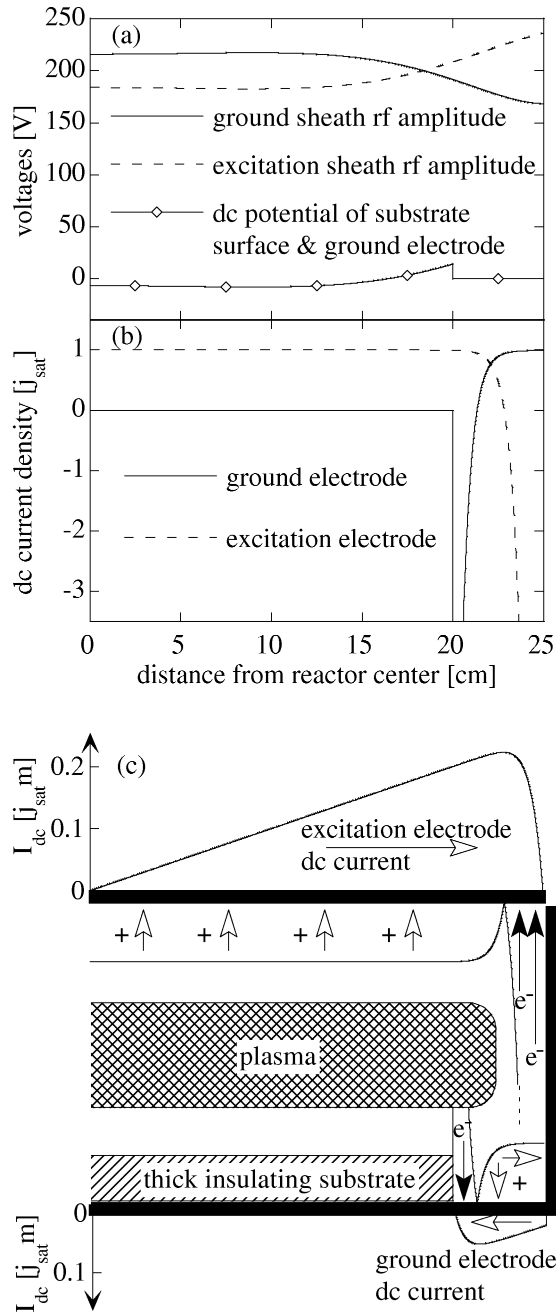

FIG. 10: For a 3 mm thick dielectric substrate ($\epsilon_r = 6$) in an asymmetric reactor: a) Sheath rf amplitude and dc potentials; b) calculated dc current flow; c) schematic representation of the dc current circulation.

$$K'_{0S} = \frac{H + F\left[H\cosh(\gamma D) + (2/\gamma)\sinh(\gamma D)\right]}{\cosh(\gamma_S S)\left[H\cosh\gamma D + (2/\gamma)\sinh\gamma D\right] + \frac{\gamma_S}{\gamma}\cosh(\gamma_S S)\left[H\sinh\gamma D + (2/\gamma)\cosh\gamma D\right]}, \tag{28}$$

$$K'_{SL} = F - K'_{0S}\cosh(\gamma_S S), \tag{29}$$

$$K''_{SL} = (\frac{\gamma_S}{\gamma})K'_{0S}\sinh(\gamma_S S). \tag{30}$$

This unwieldy solution unfortunately diminishes the illustrative value of the model. Nevertheless, it does reduce to the previous solutions in Section III A, III B and III C for S or $F \to 0$ (no, or very thin, dielectric substrate), and Section III D for $H = 0$ (no sidewalls). Depending on the dimensions, especially for thick glass, the substrate surface can be positive, despite the opposing tendency of the asymmetry effect in Section III C. In some cases, as in Fig. 10(a), the substrate surface potential (and charge) can be bipolar. The dc plasma potential of 190 V, and the self-bias of -41 V are intermediate between the cases of no substrate (section III B) and thin substrate (section III C). The similarity of the dc current flows in Figs. 8 (thin substrate) and 10 (thick substrate) shows that the effect of wall asymmetry dominates the effect of the thick glass substrate.

F. Elimination of the telegraph effect

The reactor geometry in Figs. 1 and 2 considered up till now has been the simple configuration of a plane rf excitation electrode suspended in a grounded box. If both the ground and excitation electrodes have a partial sidewall of height H_g and H_e respectively, as in Fig. III F, then the effect is to replace H everywhere by $H_g - H_e$. Clearly, if the electrode geometry were symmetric, with $H_g = H_e$ (and in the absence of a dielectric substrate), then the net sidewall rf current is eliminated, and all of the telegraph propagation non-uniformities disappear. Only evanescent fields localized at the electrode edges remain - see the next section and Figs. 13 and 15.

However, even if the sidewalls are symmetric, the electrodes should ideally *also* be symmetric from the point of view of the dielectric substrate, otherwise the telegraph effect will persist even in a symmetric reactor as shown in Section III D.

IV. NUMERICAL SIMULATIONS: TELEGRAPH EFFECT AND EDGE-LOCALIZED FIELDS

The analytical model equivalent circuit in Fig. 2 and Section III made several simplifying assumptions, such as constant sheath width, uniform plasma parameters, and a 1D approximation which treats the plasma as a flat sheet with no vertical structure. Here we consider two different numerical simulations for the plasma in two dimensions, x, z.

Maxwell's equations for an infinite, uniform plasma along y reduce to the wave equation A4 for the y-component of magnetic field. This equation was solved numerically using a commercial partial differential equation solver FLEXPDE [19]. The relative permittivity of the plasma was represented by the usual expression [12]

$$\epsilon_{pl} = 1 - \frac{\omega_{\rm pe}^2}{\omega(\omega - i\nu_m)}, \tag{31}$$

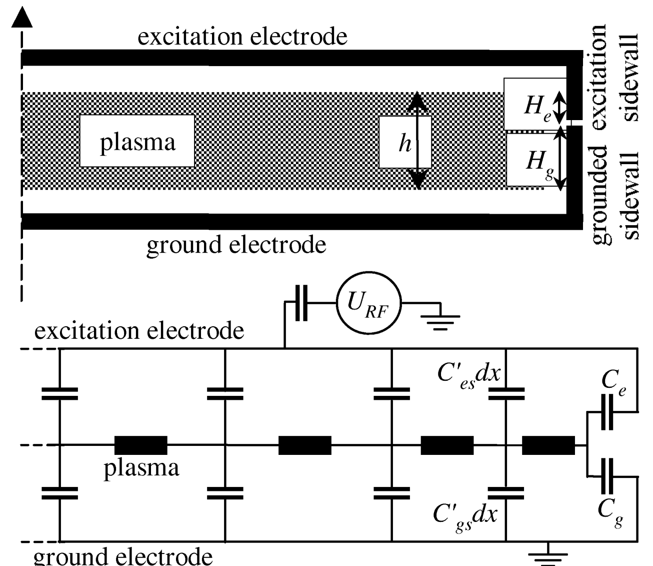

FIG. 11: Above: Schematic of the plasma reactor with partial sidewalls for both electrodes so that $h = H_g + H_e$. Below: One-dimensional representation of the plasma equivalent circuit. For the calculation of the telegraph perturbation, H is replaced by $H_g - H_e$

.

where ω_{pe}, ω and ν_m were chosen (see the caption of Fig. 12) by reference to Eq. 10 to give δ= 5 cm for comparison with the analytical model figures. The profiles of the rf amplitude of the sheath voltages and the vertically-integrated lateral current in Fig. 12(a) are the same as for the analytical solutions shown in Fig. 5. The results therefore support the 1D equivalent circuit approach in Section III. The numerical simulation also gives the vector field of the rf current, which shows the redistribution of the sidewall current to the excitation electrode in Fig. 12(b) over a distance $\sim \delta = 5$ cm. The results of the 1D telegraph model of III and Fig. 2 are therefore reproduced by the 2D Maxwell equations solution. This dielectric slab model is not a self-consistent plasma simulation and therefore it does not include the ion and electron fluxes of a plasma and so no comparison can be made here with the substrate surface voltage.

The same calculation, but for a symmetric reactor, is shown in Fig. 13. For the 1D analytical model, the case with symmetric electrodes has the trivial solution of uniform, flat profiles for the rf and dc plasma potentials as mentioned in Section III F. For the 2D calculation of a symmetric reactor, however, a perturbation of the plasma rf current in Fig. 13(b) exists near the junction of the electrodes. This is due to two sources: i) the dielectric discontinuity (impedance mismatch) at the lateral plasma/vacuum sheath transition [7]; and ii) the near field ('fringing field') of the rf power propagating into the reactor through the slit between the ground and excitation electrodes. In contrast to the propagation of the telegraph perturbation for the asymmetric

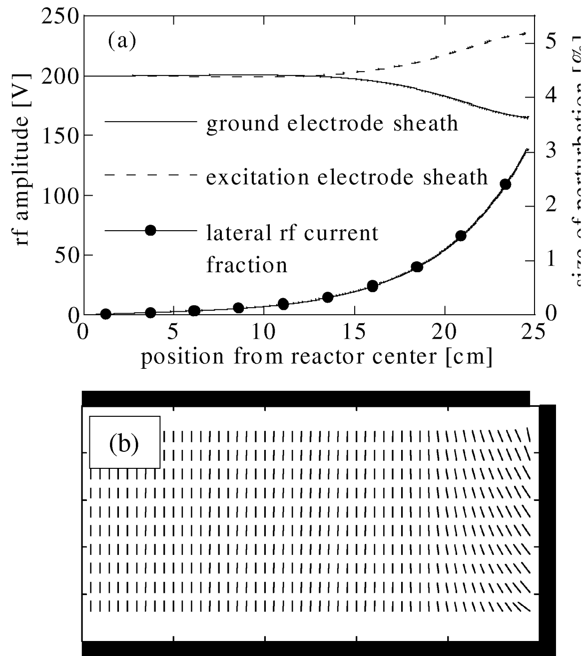

FIG. 12: a) Numerical calculation of the ground sheath rf voltage amplitude in an asymmetric reactor (with excitation frequency 13.56 MHz, $n_e = 6 \cdot 10^{15}$ m^{-3} and $\nu = 6 \cdot 10^9$ collisions per second, to give $\delta = 5$ cm), and the profile of the vertically-integrated lateral rf current; b) rf current flow pattern in the plasma showing the redistribution of the grounded sidewall current to the excitation electrode (the lateral component is magnified for clarity in the diagram).

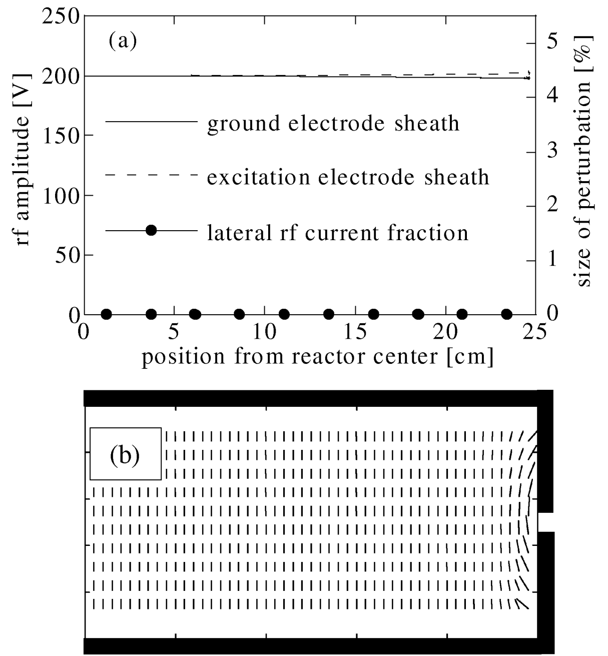

FIG. 13: The same parameters as in Fig. 12, but for symmetric electrodes: In (a), the rf perturbation is absent and there are no non-uniformities due to the telegraph effect. The rf current flow pattern in the plasma in (b) shows the closed current distribution of the grounded sidewall current to the excitation electrode (the lateral component is magnified for clarity in the diagram).

case, these perturbations are due to evanescent modes [7] which do not propagate inwards from the edge; consequently the sheath rf voltage amplitudes remain uniform and the net lateral current perturbation is zero as can be seen in Fig. 13(a). These evanescent edge effects remain even when the telegraph perturbation is removed by using symmetric electrodes, but nevertheless the consequent non-uniformity is confined to a scale length of only h/π from the reactor sidewall [7].

A more realistic self-consistent plasma simulation can be made using SIGLO-2D [20], a two-dimensional fluid model for the plasma, which self-consistently accounts for plasma density and temperature, sheath width, and fluxes of ions and electrons. The simulation ensures continuity of rf current for a resistive plasma, which suffices to demonstrate telegraph effects. In Fig. 14, the principal features of the analytical model in Section III C are reproduced, in particular, the profile of the rf potential amplitudes and the negative dc voltage of the substrate surface which would be impossible in a plasma with a unique rf plasma potential. The plasma resistivity was chosen to be similar to the value in the model. Fringing fields are also accounted for in this simulation; these fields generate an intense plasma near the junction between the rf and ground electrodes as shown by the time-averaged ionisation rate. For the asymmetric case in Fig. 14, the rf sheath voltages due to the redistribution of rf current propagating inwards causes the ionisation rate to be higher in the rf sheath for several centimeters from the edge. For the symmetric case in Fig. 15, the fringing fields still cause an intense ionisation rate in the immediate vicinity of the electrode junction at mid-height, but the rf currents are equalised at the junction and no current redistribution occurs. Therefore the rf sheath voltages, plasma power and ionisation rate are constant, as discussed in Section III F, beyond the localized fringing field zone. Comparing Figs. 14 and 15, the telegraph effect is again seen to affect the plasma uniformity over a wider edge region than the fringing field effects. Finer details of the analytical model, such as the damped oscillation in the rf amplitude profile and the exact values for the rf and dc voltages, are not reproduced because the assumptions of sinusoidal voltages and constant sheath capacitance are not valid in this self-consistent numerical simulation.

There is good agreement between the numerical simulations and the one-dimensional analytical model. The difference between the edge effects due to the telegraph propagation and the fringing evanescent fields are clearly demonstrated. The advantage of the analytical approach for the telegraph model is the understanding given by the physical interpretation.

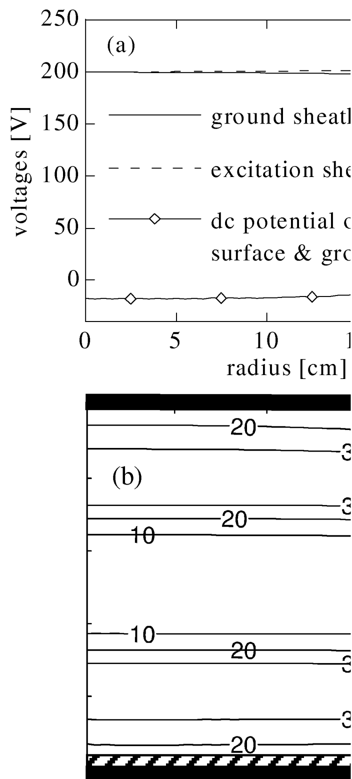

FIG. 14: 2D fluid simulation (SIGLO-2D) for a cylindrical reactor: (a) profile of the rf potential amplitude across the electrode sheaths, and the dc surface potential, with a thin dielectric substrate ($\epsilon_r = 6$, 0.5 mm thick), as in Section III C. Note that the details of the damped oscillation in rf amplitude are absent, although the principal features remain. Also, the negative substrate potential in Fig. 8(a) is confirmed; (b) contour plot of the time-averaged ionisation rate in the electrode gap.

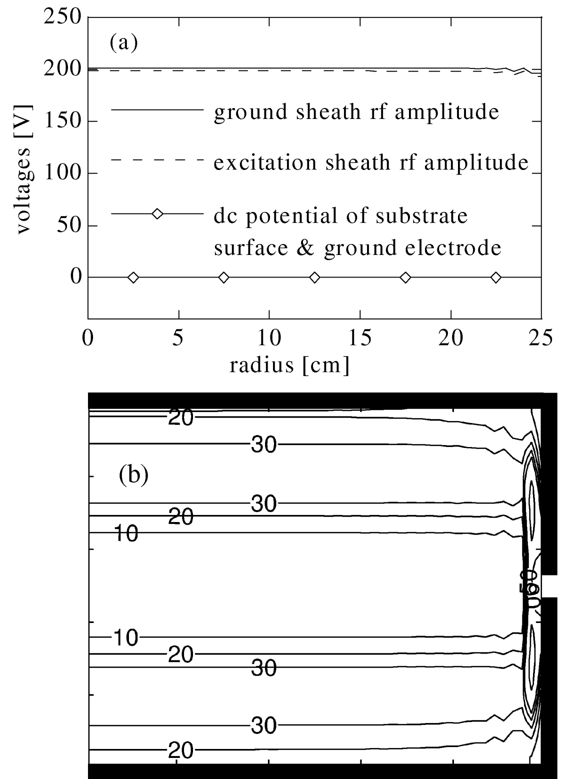

FIG. 15: 2D fluid simulation (SIGLO-2D) as in Fig. 14 but for symmetric electrodes; (a) the rf perturbation is absent and there are no non-uniformities due to the telegraph effect; (b) the ionisation rate is highest near the electrode junction at mid-height due to the localized fringing fields.

V. CONSEQUENCES OF THE NON-UNIFORM RF PLASMA POTENTIAL DUE TO THE TELEGRAPH EFFECT

Some consequences of the telegraph model are summarised for an asymmetric reactor (with rf electrode smaller than ground electrode) for plasma conditions so that $\delta < L$. The telegraph model predicts that:

i) The rf plasma potential and sheath rf voltages vary across the reactor. The net rf power dissipation is therefore non-uniform, with the plasma becoming more intense near to the edges. In contrast, an intense edge plasma due to fringing fields [7] is confined to the immediate vicinity of the edge discontinuities. In the examples shown, the variations in rf power due to the telegraph effect are only a few per cent if summed for both sheaths, but they are much larger for each individual sheath.

ii) For a sufficiently thin substrate, the substrate surface potential and charge are negative and non-uniform across the substrate, and not only positive and uniform. Negative substrate charging has been observed experimentally [13]. For a sufficiently thick substrate, the surface potential can become positive or even bipolar. Non-uniform dc potential on the substrate surface in the presence of a uniform dc plasma potential results in non-uniform ion bombardment energy, which is detrimental for some plasma processes.

iii) The self-bias is different from that estimated using the conventional 'area law'. For example, it depends on the plasma parameters and the dimensions of the reactor. It becomes more negative for a thin dielectric substrate partially covering the ground electrode.

iv) Dc current circulates internally, via the plasma across the sheath and returns along the electrode conducting surfaces. This distribution of dc current flow across the sheaths has been observed experimentally [14]. A localised peak of electron flux from the plasma can arise at the edge of a substrate and also at the edge of the excitation electrode.

If the reactor configuration, including substrates, is symmetric, then all of the telegraph propagation non-uniformities disappear, leaving only the fringing evanescent fields localized at the electrode edges.

VI. CONCLUSIONS

An analytical model and numerical simulations show that electrode edge asymmetry in rf plasma reactors causes a spatial variation in the rf plasma potential which can be described by a telegraph equation. This leads to non-uniform rf sheath voltages and rf power density in the reactor which would perturb the process uniformity. The non-uniform rf plasma potential in presence of the uniform dc plasma potential results in non-ambipolar currents circulating through the plasma and along conducting electrode surfaces. Another consequence is that the surface potential of a dielectric substrate can be negative. The dc sheath potential can vary over a dielectric substrate resulting in non-uniform ion bombardment energy. If the electrode sidewall areas are made equal, then the rf plasma potential and the power density are made uniform, except for localized fringing fields due to edge discontinuities.

Acknowledgments

This work was funded by Swiss Federal Research Grant CTI 5994.2 and performed with the collaboration of Unaxis Displays in Palaiseau, France, and Truebbach, Switzerland.

APPENDIX A: THE COMBINATION OF TELEGRAPH, STANDING WAVE AND EDGE-LOCALIZED EFFECTS

In the first part of this work it was assumed that the rf frequency was low enough such that a quarter rf wavelength was much longer than the reactor dimensions. Finite wavelength (standing wave) effects associated with high frequencies in large reactors [4–9] were therefore absent and any non-uniformity of the plasma rf potential was due solely to the telegraph effect in the analytical model. In this appendix, we briefly consider the different origins of the telegraph, standing wave and edge-localized effects.

For the case of a reactor infinitely long and uniform along y, the electromagnetic propagation mode along x is a quasi-TEM mode, having only the magnetic field component H_y, since the excitation frequency used is far below the cutoff frequency of the first TM mode [9]. Maxwell's equations can be written for the co-ordinate system in Fig. 1 as:

$$\frac{\partial H_y}{\partial z} = -i\omega\epsilon_0\epsilon_r(x,z)E_x, \tag{A1}$$

$$\frac{\partial H_y}{\partial x} = i\omega\epsilon_0\epsilon_r(x,z)E_z, \tag{A2}$$

$$\frac{\partial E_x}{\partial z} - \frac{\partial E_z}{\partial x} = -i\omega\mu_0 H_y, \tag{A3}$$

where $\epsilon_r(x,z) = 1$ in the vacuum sheath region, and $\epsilon_r(x,z) = \epsilon_{pl}$ (see Eq. 31) for the plasma. The field equation for H_y is therefore

$$\frac{\partial}{\partial x}\left[\frac{1}{\epsilon_r(x,z)}\frac{\partial H_y}{\partial x}\right] + \frac{\partial}{\partial z}\left[\frac{1}{\epsilon_r(x,z)}\frac{\partial H_y}{\partial z}\right] + k_0^2 H_y = 0, \tag{A4}$$

where $k_0 = \omega/c$ is the vacuum wave number of the rf excitation. The combination of the standing wave, telegraph and edge-localized effects all appear in the solution for this field equation for the asymmetric geometry of Fig. 2. The correspondence between the plasma complex conductivity σ_{pl} in Section III and the relative permittivity ϵ_{pl} of the plasma can be seen from the equivalent expressions in Maxwell's equation for $\nabla \wedge \underline{H}$:

$$\nabla \wedge \underline{H} = j\omega\epsilon_0\epsilon_{pl}\underline{E} = (\sigma_{pl} + j\omega\epsilon_0)\underline{E}. \tag{A5}$$

The telegraph effect appears as a natural mode in Eq. A4 (as will be shown in a separate paper) which propagates inwards from the edge, as described in Section III. The solution in Refs. [7] and [21] is for a symmetric reactor and therefore does not include the telegraph effect. For the collisional plasmas considered in this work, the resistive skin depth

$$\delta_{\text{resistive}} = \sqrt{\frac{2}{\omega\sigma_{dc}\mu_0}}, \tag{A6}$$

is much longer than the plasma slab height h (and longer than the telegraph damping length, δ), and so it was justified, in retrospect, to treat the plasma as a uniform conductor for the telegraph effect in Section III. Edge discontinuities (see Section IV) give rise to edge-localized evanescent modes of scale length h/π [7] which do not propagate.

In this appendix, the interest in separating the standing wave and telegraph effects, insofar as their superposition gives a reasonably accurate representation of the full solution, is to obtain an understanding of the physical cause of each phenomenon. Once identified, steps can be taken to eliminate each source of non-uniformity. The surface wave mode, which gives rise to the standing wave effect, and the telegraph mode can be compared using their equivalent circuit descriptions. The equivalent circuit for the surface wave can be represented as in Fig. 16, where the rf excitation voltage propagates along the electrodes which are separated by a dielectric medium consisting of the plasma/sheath series combination. For the telegraph effect, Fig. 2 shows the perturbation propagating inwards along the lossy plasma, with the vacuum sheaths providing the dielectric separation of the resistive plasma from the electrodes. It is the transmission along the lossy plasma which causes the telegraph wavelength and damping length to be much shorter than for the surface wave.

Any non-uniform plasma rf potential, whether due to telegraph, standing wave or both effects simultaneously, in presence of a uniform plasma dc potential, will give

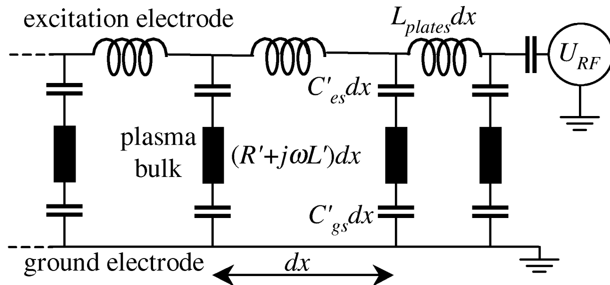

FIG. 16: A one-dimensional equivalent circuit for the propagation of the surface wave. L_{plates} represents the self-inductance per square of the parallel plate electrodes, and $R' + j\omega L'$ represents the transverse bulk plasma impedance per unit area.

rise to dc currents circulating via the plasma and conducting electrode surfaces; preliminary experiments have measured these dc currents in all of these cases [14].

REFERENCES

[1] H. Meiling, W. G. J. H. M. van Sark, J. Bezemer, and W. F. van der Weg, J. Appl. Phys **80**, 3546 (1996).

[2] L. Sansonnens, J. Bondkowski, S. Mousel, J. P. M. Schmitt, and V. Cassagne, Thin Solid Films **427**, 21 (2003).

[3] C. Hollenstein, A. A. Howling, C. Courteille, J.-L. Dorier, L. Sansonnens, D. Magni, and H. Müller, Mat. Res. Soc. Symp. Proc. **507**, 547 (1998).

[4] J. P. M. Schmitt, Thin Solid Films **174**, 193 (1989).

[5] J. P. M. Schmitt, Mat. Res. Soc. Symp. Proc **219**, 631 (1992).

[6] L. Sansonnens, A. Pletzer, D. Magni, A. A. Howling, C. Hollenstein, and J. P. M. Schmitt, Plasma Sources Sci. Technol. **6**, 170 (1997).

[7] M. A. Lieberman, J. P. Booth, P. Chabert, J. M. Rax, and M. M. Turner, Plasma Sources Sci. Technol. **11**, 283 (2002).

[8] L. Sansonnens and J. Schmitt, Appl. Phys. Lett. **82**, 182 (2003).

[9] H. Schmidt, L. Sansonnens, A. A. Howling, C. Hollenstein, M. Elyaakoubi, and J. P. M. Schmitt, J. Appl. Phys. **95**, 4559 (2004).

[10] J. P. M. Schmitt, M. Elyaakoubi, and L. Sansonnens, Pl. Sources Sci. Technol. **11**, A206 (2002).

[11] K. Köhler, J. W. Cobrun, D. E. Horne, E. Kay, and J. H. Keller, J. Appl. Phys. **57**, 59 (1985).

[12] M. A. Lieberman and A. J. Lichtenberg, *Principles of Plasma Discharges and Materials Processing* (John Wiley and Sons, New York, 1994).

[13] A. A. Howling, A. Belinger, P. Bulkin, L. Delaunay, M. Elyaakoubi, C. Hollenstein, J. Perrin, L. Sansonnens, J. Schmitt, and E. Turlot, Proc. 15th Int. Symp. Plasma Chemistry, Orleans, France **1**, 33 (2001).

[14] J. Ballutaud, C. Hollenstein, A. A. Howling, L. Sansonnens, H. Schmidt, and J. P. M. Schmitt, Proceedings of the 16th Int. Symp. Pl. Chem. ISPC16, June 22-27 (2003), Taormina, Italy, CD-ROM published by the Organizing Committee, edited by R. D'Agostino, Dipartimento di Chimica, Universita degli Studi di Bari, 70126 Bari, Italy.

[15] K.-U. Riemann, J. Appl. Phys. **65**, 999 (1989).

[16] A. Garscadden and K. G. Emeleus, Proc. Phys. Soc. **79**, 535 (1962).

[17] H. S. Butler and G. S. Kino, Phys. Fluids **6**, 1346 (1963).

[18] D. Herrebout, A. Bogaerts, M. Yan, R. Gijbels, W. Goedheer, and A. Vanhulsel, J. Appl. Phys. **92**, 2290 (2002).

[19] Available from http://www.pdesolutions.com.

[20] J. P. Boeuf and L. C. Pitchford, Phys. Rev. E **51**, 1376 (1995).

[21] P. Chabert, J. L. Raimbault, J. M. Rax, and M. A. Lieberman, Phys. Pl. **11**, 1775 (2004).